CBN 96-1
A. Temnykh and D.Rubin
January 9, 1996

Effect of Q1-Q2 and REC vacuum chamber welds on dynamic aperture

1 Introduction

Stainless steel (SS), well known as a good non magnetic material, was used for building CESR's IR vacuum chambers. Non magnetic filler was used to weld the sections together.

One of IR vacuum chambers, the Q1-Q2 pipe was made by squashing a cylindrical SS pipe. It is shown in Figure 1. Copper pipes are welded onto the edges to provide cooling. After assembly of the interaction region vacuum system it was found that some regions near the cooling tubes have permeability as high as 1.3 as compared to a typical value for stainless steel of 1.02. This prompted an exploration of the associated distortion of the magnetic fields of the IR quads by the welded vacuum chambers, and the effect of the resulting nonlinear fields on CESR beam dynamics.

2 Welds

To estimate the magnetic field perturbation in the region of the welds we cut a small section from the Q1-Q2 prototype vacuum chamber, placed it in a uniform dipole magnetic field, B=1647 Gauss, and measured with a hall probe the field perturbation around the piece. The tested piece is shown in Figure 2. The first photograph is a view from the outside. It shows a section of vacuum chamber and the cooling pipe welded to it. The second picture shows the internal suface. Non uniformity of the weld is evident. There is an overheated region that is indicated by discoloration of the surface. It is marked by "1". Label "2" marks a normal, non overheated region. Measurements with a permeability meter show the biggest change of permeability near region "1".

The field was measured as shown in Figure 3. The results of the magnetic measurements are presented in Figure 4. The field is measured as a function of horizontal positon at three different positions along the length of the pipe; directly over the overheated region (Section 1), directly over the softly heated region (Section 2), and over a section of chamber that had no weld. The difference of the measured field and unperturbed field is plotted for each of the three cases. The curve labeled "Stability study" corresponds to the difference of two measurements under identical conditions and indicates the resolution and quality of the measurement.

The biggest effect, as anticipated, is in the scan around the overheated region, see "Section 1" plot. It is consistent with the permeability meter measurements mentioned above. "Section 2", which is a scan around the softly heated location, and "Section 3" for the sample without the weld give a similar level of field distortion. The effect indicated by the "Section 3" plot is presumably the result of a change in magnetic permeability due to the mechanical stress of the material. In our case, the measurement with the permeability meter shows that bending the stainless steel pipe changed its permeability from 1.014 to 1.042. The similarity of the "Section 2" and "Section 3" measurements indicates that the field distortion around the softly heated region is caused not by the weld but simply the mechanical stress at the bend.

We conclude that welded stainless is acceptable in the manufacture of vacuum chambers if overheating can be avoided.

The next step was the simulation of the result of the above measurents with the POISSON program. We found that the worst case distortion of the magnetic field and corresponding to the "Section 1" plot can be modeled as a 3x3mm long bar with magnetic permeability μ equal to 2. Figure 5 shows a comparison between the resulting model and the measurements.

In order to develop an analytical formula for the magnetic field pertur-

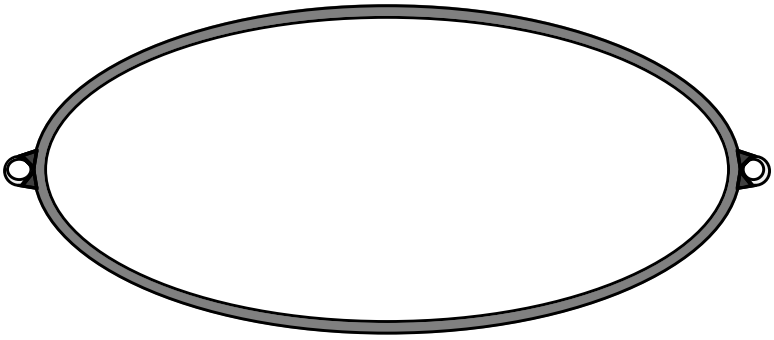

Figure 1: Q1-Q2 vacuum chamber profile. Cooling tubes are welded onto both sides of the chamber.

Figure 2: Tested piece of Q1-Q2 vacuum chamber. The first picture is a view of the outside, and the second shows the internal surface.

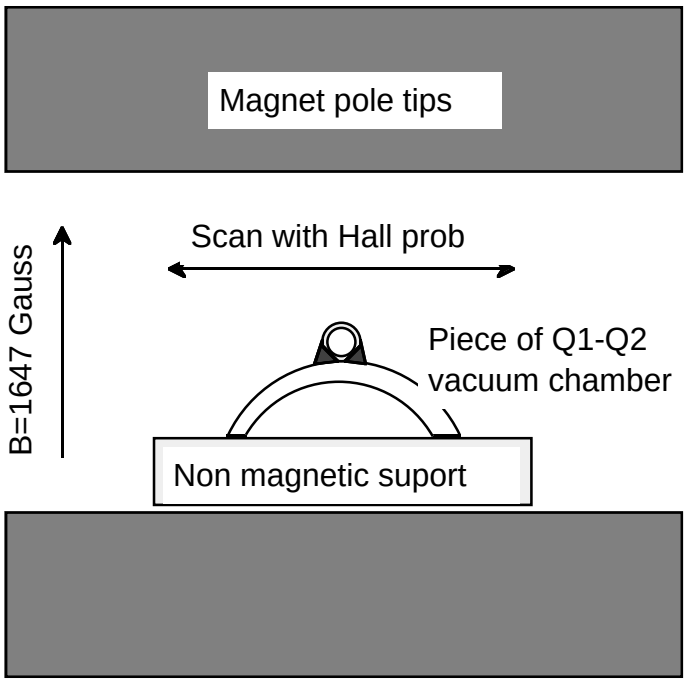

Figure 3: Measurement of the magnetic field distortion around the weld.

Figure 4: Vertical magnetic field perturbation. "Stability study" difference between two similar measurements. "Section 1" field distortion around hard heated region. "Section 2" is around soft heated location. "Section 3" scan around example without weld.

Figure 5: Comparison between measured field perturbation and calculated for 3x3mm rod with $\mu = 2$.

bation in the Q1 and Q2 magnets, we started from expressions for magnetic field of a long thin wire with current, then used the software "Mathematica" for Macintosh to evaluate it in the case of two long magnetic dipoles polarized in opposite directions and located at coordinates $\pm d$ in the horizontal plane, where d is the half width of the vacuum chamber. The resulting fields are given by

$$B_x = \frac{2\,b0\;(-d+x)\;y}{\left((-d+x)^2+y^2\right)^2} - \frac{2\,b0\;(d+x)\;y}{\left((d+x)^2+y^2\right)^2}$$

$$B_y = \frac{b0\;\left(-(-d+x)^2+y^2\right)}{\left((-d+x)^2+y^2\right)^2} - \frac{b0\;\left(-(d+x)^2+y^2\right)}{\left((d+x)^2+y^2\right)^2}.$$

Here B_x, B_y are the horizontal and vertical components of field, and $b0$ is the parameter proportional to the strength of the perturbation. Note that the final expressions satisfy Maxwell's equations and are consistent with the POISSON calculation.

The same technique was used to calculate the magnetic field perturbation caused by the welded vacuum chamber in the REC quad region. Here the round vacuum chamber contains four long welds configured as shown in

Figure 6: Perturbation of magnetic field calculated with POISSON program. a) One quarter of Q1-Q2 quads. Region with highest density of magnetic lines shows the weld location. b) REC magnet. Four regions with high magnetic line density are weld locations on the round REC vacuum chamber.

Figure 6b. In this case, in the model for calculation of the magnetic field, the welds are represented by four long magnetic dipoles.

The structure of the perturbation of the magnetic field in both cases, Q1 - Q2 and REC, calculated by the POISSON program is shown in Figure 6.

3 Dynamic Aperture

The effect of the nonlinear distortion of magnetic fields generated by the chamber welds in the Q1 and REC quads is explored by a tracking study. The transverse kicks due to the perturbed fields, as per the model developed above, are shown in Figures 7 and 8.

The model of the storage ring optics is based on the current crossing angle conditions. The linear optics are N9A19C501.FD93S_4S. The design sextupole distribution is used so that the chromaticities and tonalities are unity and zero respectively. The horizontal and vertical separators are included so that the closed orbit mimics real conditions. East and west RF cavities, with 3MeV peak voltage, apply an energy kick that is proportional to longitudinal displacement from the synchronous orbit. As a result, all

manner of nonlinear transverse and synchrobetatron resonances can and do appear in a scan of the tune plane.

A trajectory is stable if its amplitude has not increased after 1000 turns. The dynamic aperture is the largest stable transverse amplitude. The largest stable transverse amplitude for ΔE, and $\Delta E = 10\sigma_E$ is indicated in Figure 9 for the machine with perfect quadrupole and sextupole fields. The transverse coordinate of the trajectory at the interaction point is shown in the plot. The inner and outer boxes about the origin indicate 7.5σ and 10σ transverse displacements respectively. The vertical beam size is based on a vertical emittance equal to half of the horizontal emittance. The horizontal emittance is $\epsilon_h = 0.2mm - mrad$. Note the near energy independence of the dynamic aperture in the design optics. The dynamic aperture is reduced by the nonlinearities due to the welds as indicated in Figure 10. The integrated kicks associated with the chamber welds within Q1 and the REC are divided in half and included as thin elements at each end of the corresponding magnet in an attempt to distribute the fields. Since the cooling channel is epoxied rather than welded to the Q1 east chamber, the nonlinear kicks appear only adjacent to Q1 west.

There is a significant reduction in the maximum stable horizontal amplitude as a result of the weld induced nonlinearities. The energy independence of dynamic aperture in the ideal optics is also compromised.

In the case of the ideal optics, the nonlinear aperture is well outside of the physical aperture of the machine. The maximum stable amplitude in the

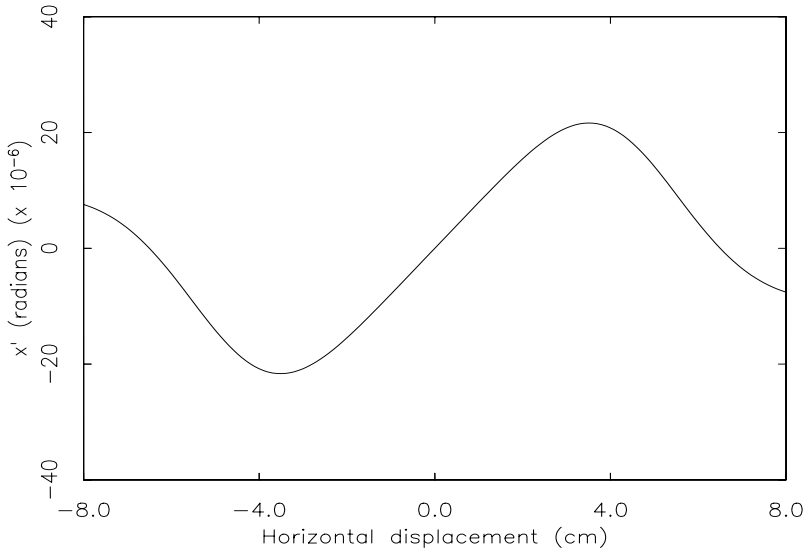

Figure 7: The integrated transverse kick for the REC due to the non-unity permeability of the chamber welds.

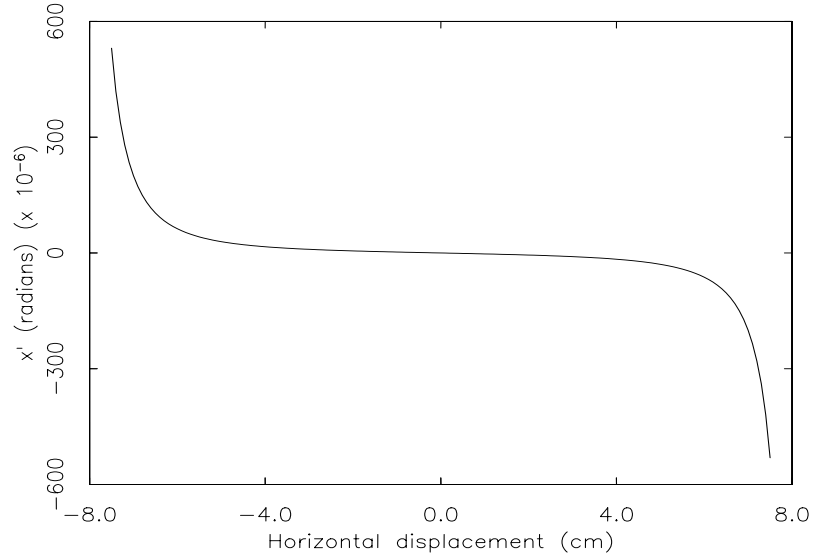

Figure 8: The integrated transverse kick for Q1 due to the non-unity permeability of the chamber welds.

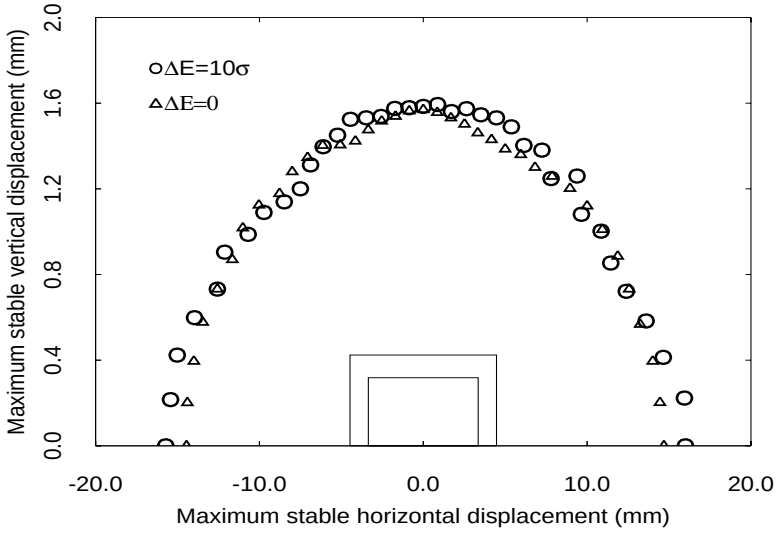

Figure 9: The dynamic aperture in the design quadrupole and sextupole optics with no quadrupole nonlinearities.

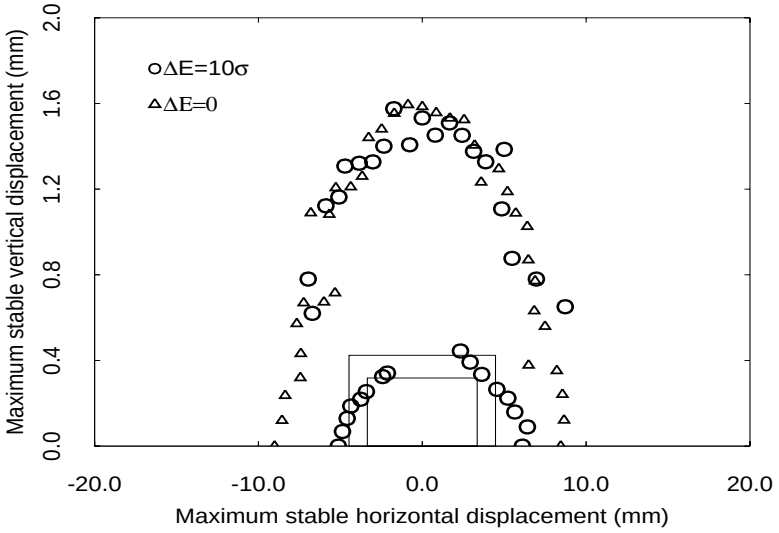

Figure 10: The dynamic aperture with REQ, and Q1 west fields modified as shown in Figures 1 and 2 respectively.

machine with ideal quadrupole and sextupole optics and with real physical apertures is shown in Figure 11.

If the weld induced nonlinearities in the REQ and Q1 west are included we compute the maximum stable aperture that is shown in Figure 12. The dynamic aperture is indeed reduced by the weld nonlinearities, but is nevertheless greater than the physical aperture for on energy particles and roughly the same as the physical aperture for off energy trajectories.

Therefore one might conclude that the welds do not impact machine performance. And if these were the only nonlinearities in the machine that might be a fair conclusion. It is much more difficult to estimate the combined effect of the nonlinearities included in the simulation, and those that are not, and especially those due to the beam-beam interaction. Furthermore, the tracking excercise described above is at a particular betatron tune. The effect of the welds on dynamic aperture presumably depends on tune and their presence almost certainly narrows the good operating region of the tune plane.

For a given intial amplitude, the maximum amplitude that obtains in the course of several hundred turns depends on the betatron tune. The tune dependence of the amplitude for the ideal machine is shown in Figure 13. The initial amplitude for the trajectory is $6\sigma_x = 3.2mm$,$6\sigma_y = 60\mu m$, and $6\sigma_E/E = 3.6 \times 10^{-3}$ The contours indicate tunes where the particle amplitude is increasing from the nominal 6σ. Particles with horizontal amplitude greater than about $6\sigma_x$ will be lost due to interaction with the core of counter-

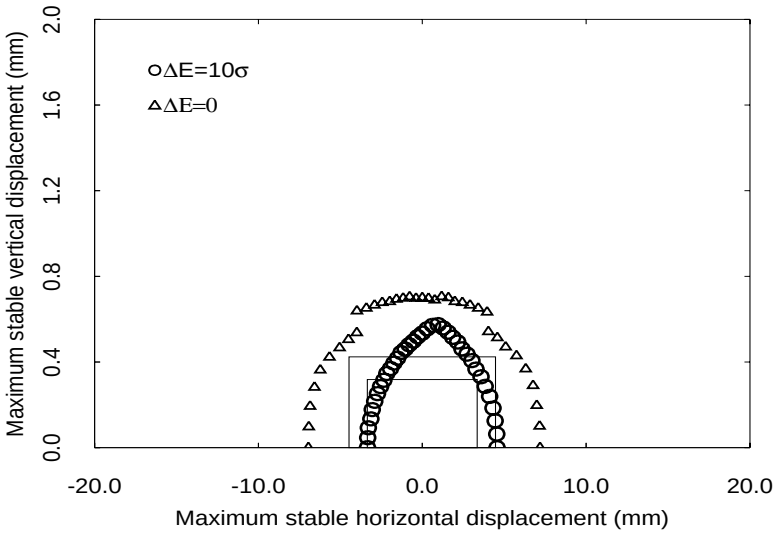

Figure 11: The maximum stable amplitude in the design optics with real physical apertures and no quadrupole nonlinearities.

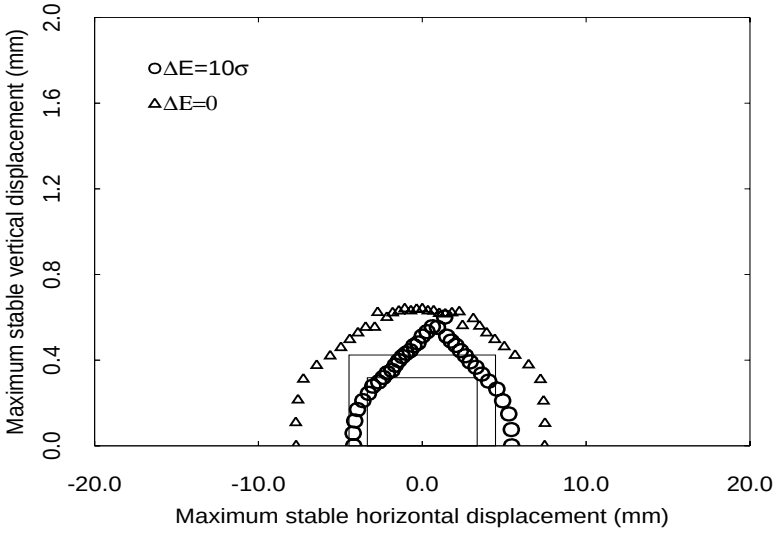

Figure 12: Maximum stable amplitude including weld nonlinearities and real physical aperture.

rotating bunches and at 7.5 to $8\sigma_x$, particles will strike the vacuum chamber walls at the pretzel peaks in the arcs. Increase in vertical amplitudes will contribute to vertical tails which will eventually limit beam-beam tune shift. In the plot of horizontal amplitudes the synchro-betatron resonance lines $2Q_x - 2Q_s = n$, $2Q_x - 4Q_s = n$, and $2Q_x - 6Q_s = n$ are apparent. In the plot of vertical amplitudes we see the coupling resonance ($Q_y - Q_x = n$) and the synchrotron sideband ($Q_y - Q_x - Q_s = n$).

If the nonlinearities due to the welds are included, resonance widths are enhanced, especially the synchro-betatron line $2Q_x - 2Q_s$, as can be seen in Figure 14. Any reduction in the stable operating area may limit achievable beam-beam tune shift.

We also consider permanent magnet weld induced nonlinearities and those associated with Q1 west separately. If we assume that the permeable welds in the Q1 chamber are eliminated, and that the REC chambers are unchanged, then we compute the dynamic aperture (in the absence of a physical aperture constraint) that is shown in Figure 15. The dyamic aperture shown in Figure 15 (REC chamber welds only) is to be compared with Figure 10 (REC chamber welds and Q1 west chamber welds) and Figure 9 (no weld nonlinearities). We find that replacement of the Q1 west chamber with welded cooling channel by something like the Q1 east chamber with epoxied cooling channel would yield a significant increase in the maximum stable amplitude.

4 Conclusions

The field nonlinearities in Q1 and the REC due to the permeable welds reduces dynamic aperture. The scan of the tune plane indicates that while stable regions exist, the width of various resonances is increased. Repair of the west Q1-Q2 chamber would significantly improve the dynamic aperture.

5 Acknowledgement

Thanks to Dave Rice for directing our attention to the effects of welded chambers.

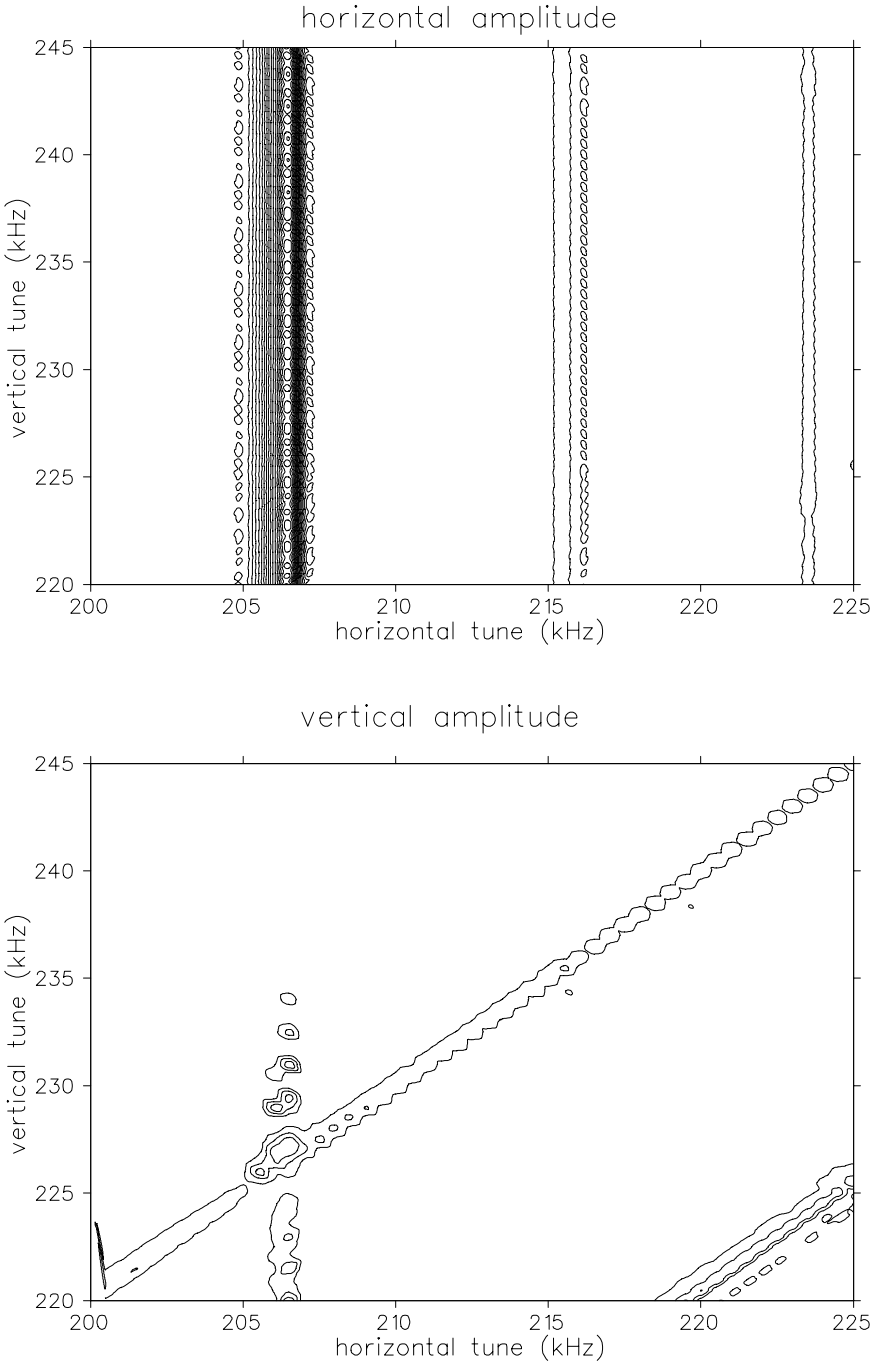

Figure 13: Horizontal and vertical amplitudes respectively as a function of transverse betatron tune in the ideal machine.

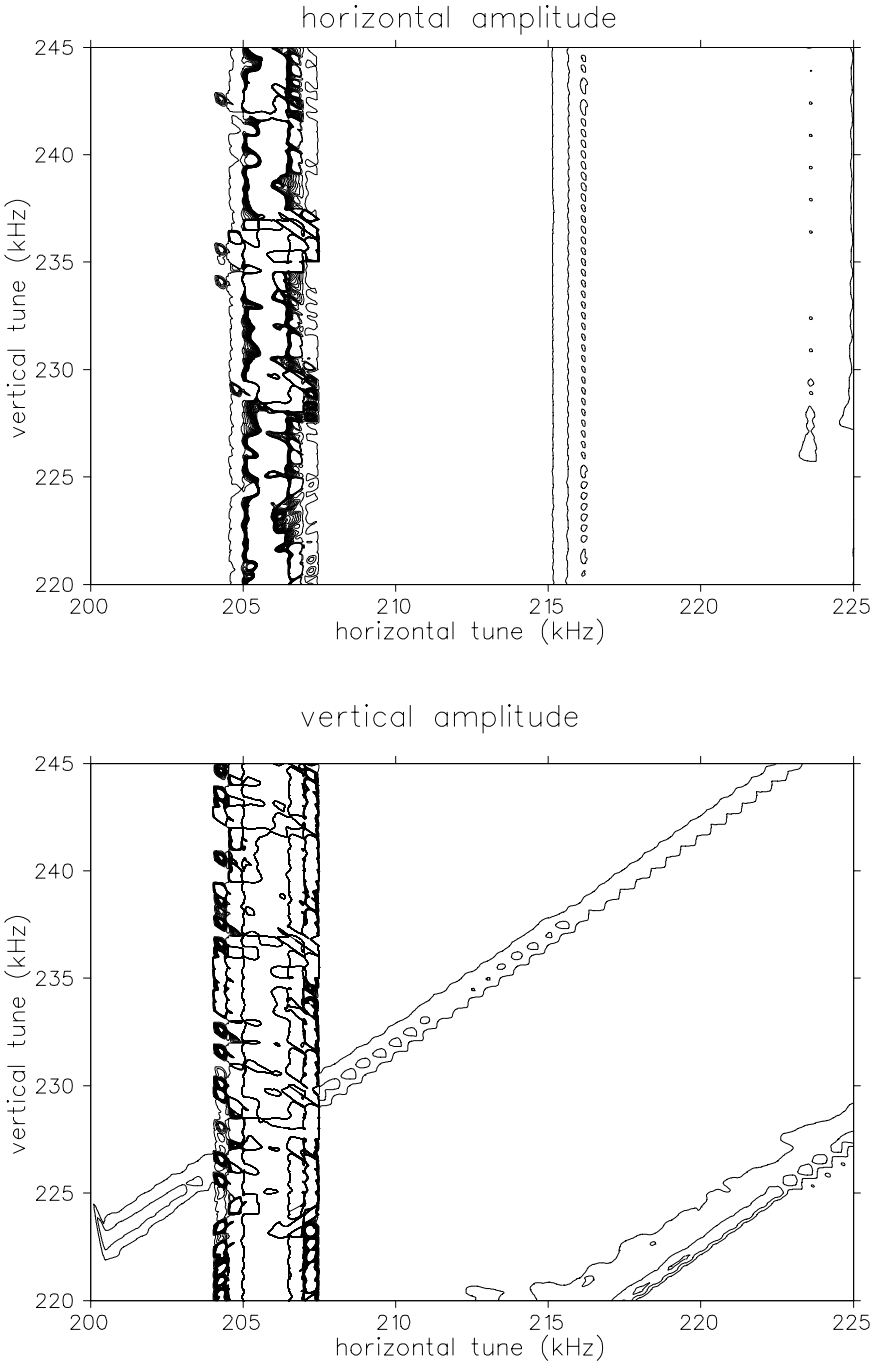

Figure 14: Horizontal and vertical amplitudes respectively as a function of transverse betatron tune in the machine with weld nonlinearities.

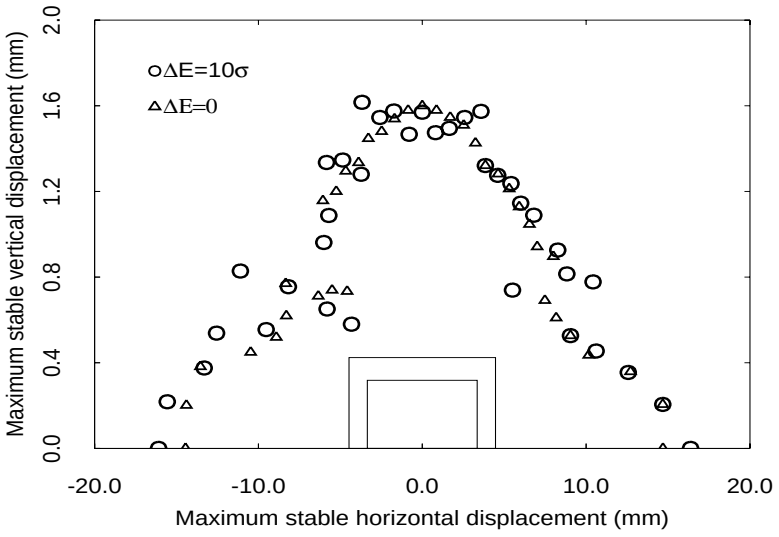

Figure 15: The maximum stable amplitude REC nonlinearity but no Q1 nonlinearity. The physical aperture is assumed to be very large.